

## Seismic cycle and plate margin deformation in Costa Rica: GPS observations 1994-1997

P. Lundgren<sup>1</sup>, M. Protti<sup>2</sup>, A. Donnellan<sup>1</sup>, M. Heflin<sup>1</sup>, E. Hernandez<sup>2</sup>, and D. Jefferson<sup>1</sup>

<sup>1</sup>Jet Propulsion Laboratory, California Institute of Technology, Pasadena

<sup>2</sup>OVSICORI, Universidad Nacional, Heredia, Costa Rica

**Abstract:** GPS observations in Costa Rica from 1994-1997 reveal a complex pattern of motion consistent with the superposition of seismic cycle and secular plate margin deformation. In the south, velocity vectors are consistent with motion of the Panama Block plus postseismic deformation following the 1991 Limon earthquake, and interseismic strain due to partial locking of the Middle America Trench (MAT) thrust. In the northwest, sites west of the volcanic arc are moving to the NW as a forearc sliver. Superimposed on this sliver motion are vertical and horizontal interseismic deformations from the adjacent Nicoya segment of the MAT. We apply two different inverse methods to understand the source of the seismic strain in NW Costa Rica. We compare fault locking models derived using a singular value decomposition inversion with that of a simulated annealing global optimization approach. Both methods yield similar models for partial locking of the thrust interface beneath the Nicoya Peninsula. Our results define an area of nearly fully locked fault beneath the outer coast of the southern portion of the peninsula, with somewhat lower coupling beneath the northern half, and with low coupling elsewhere. These initial results show the promise for detailed imaging of the locked portion of a thrust interface responsible for future large subduction zone earthquakes.

### Introduction

Costa Rica lies in a complicated tectonic setting featuring fast subduction, deformation of the Caribbean Plate margin, recent large earthquakes (Fig. 1), and the unusual location of the Nicoya Peninsula, which lies near the Middle America Trench (MAT) directly above the seismogenic zone of the subduction underthrust [Mann *et al.*, 1990]. Off the southwest coast of Costa Rica the

Cocos plate subducts along the MAT at a convergence rate of 86-92 mm/yr [DeMets *et al.*, 1994]. Along its southeast Caribbean coast lie the thrust faults of the North Panama Deformed Belt (NPDB), recently the location of the 1991  $M_w$  7.6 Limon earthquake [Plafker and Ward, 1992]. The NPDB becomes a shear zone that cuts inland across central Costa Rica and forms the northern boundary of the Panama Block [Protti and Schwartz, 1994]. Off the northwest Pacific coast, immediately NW of the Nicoya Peninsula, the 1992  $M_w$  7.6 Nicaragua tsunamigenic earthquake ruptured the upper portion of the subduction thrust [Kanamori and Kikuchi, 1993; Piatanesi *et al.*, 1996; Ihmle, 1996]. In 1990 a  $M_w$  7.0 thrust event occurred directly SE of the Nicoya Peninsula [Protti *et al.*, 1995a]. This contrasts with the Nicoya segment, which lies between these two recent earthquakes and is currently seismically quiescent but has been the location of earthquakes with  $M > 7.5$  as recently as 1950. The Nicoya Peninsula's unusual topography and long-term measured uplift and subsidence pattern are consistent with strong seismic coupling beneath it, and repeated large earthquakes that rupture the length of the peninsula [Marshall and Anderson, 1995].

The CORI GPS project was initiated in 1991 to address questions of seismic cycle deformation and plate margin deformation. It built upon measurements of coseismic displacements of the Limon earthquake in 1991 over a sparse GPS network [Lundgren *et al.*, 1993] with a specific goal of targeting the Nicoya segment, both because of its maturity in the earthquake cycle and because of the proximity of the Nicoya Peninsula to the trench, allowing much higher resolution of the distribution of slip over the seismogenic portion of the subduction thrust.

We present GPS solutions from the CORI network from 1994-1997. We find a spatiotemporal pattern of deformation that is consistent with the expected secular plate margin motions and a superimposed pattern of earthquake cycle deformation. In particular, we invert for elastic deformation due to slip on the thrust interface of the MAT off northwest Costa Rica. We find that a combination of trench parallel motion of the forearc and interseismic strain due to heterogeneous partial locking beneath the Nicoya Peninsula are required to model the GPS derived velocities.

## GPS Analysis

We measured site positions by analyzing data from dual frequency GPS receivers. Observations were carried out from 3-5 days for most sites (some up to 2 weeks), with all sites measured in February 1994 and 1996. Twelve sites in NW Costa Rica were measured a third time in April 1997. Data from 1994 and 1996 were collected with Turborogue receivers using Dorn-Margolin choke-ring antennas. Data from the 1997 survey were split between Turbo rogues and Trimble 4000SSi receivers, with both types using choke-ring antennas to minimize systematic errors due to heterogeneous receivers and antennas.

We analyzed the GPS data using the GIPSY/OASIS II software [*Lichten and Border, 1987; Webb and Zumberge, 1995; Zumberge et al., 1997*]. We used the precise orbits and clocks provided by the Jet Propulsion Laboratory, employing a reference-frame-free strategy [*Heflin et al., 1992*] and correcting for carrier phase ambiguities [*Blewitt, 1989*]. Each of these daily network solutions were then transformed into the ITRF94 reference frame [*Zumberge et al., 1997*]. All the daily solutions were combined to derive site positions and velocities using a weighted least squares inversion that is part of the GIPSY/OASIS II software. For each station outlying daily solutions were removed (usually due to a short occupation interval on the first or last UTC day or due to noisy data). The affected daily network solution was then reanalyzed and the site velocities recombined. For the final set of combined solutions the reduced chi-squared value was 13.49, suggesting that the calculated formal errors are too low. The data covariances were scaled by 13.49 to lower the reduced chi-squared to one, which is equivalent to scaling the solution errors by 3.67.

The final rates and their scaled one sigma errors are given in Table 1. Horizontal rate uncertainties are generally one to several mm/yr, while vertical rate uncertainties are from five to more than ten mm/yr, and are similar in magnitude to campaign measurements found over a similar time period in Alaska [*Freymueller et al., 1999*]. Several representative station time series are plotted (in ITRF94 reference frame) to give a feel for the velocity solutions (Fig. 2). The examples shown are for sites in the Nicoya region, although sites in other parts of Costa Rica give similar solutions but without any data in 1997.

To convert horizontal velocities relative to a fixed Caribbean plate (Fig. 3a), we used a model for the rotation of the Caribbean plate relative to ITRF94 [Dixon *et al.*, 1998]. This model is based on GPS solutions for two sites assumed to be on the stable Caribbean plate (SANA, San Andreas Island; ROJO, Dominican Republic). The site ACOS is the site within the Costa Rica network that is most likely to lie on stable Caribbean lithosphere (or at least have the least amount of motion relative to that plate). We found it to have a very small motion directed away from the Middle America Trench, suggesting that the model of Dixon *et al.* [1998] provides a reasonable fit to this part of the Caribbean plate.

The horizontal velocities show distinct patterns of motion relative to the Caribbean plate. Across the Nicoya Peninsula, directly outboard of site ACOS, sites on the outer central Pacific coast side of the peninsula have high velocities towards the NE away from the MAT which decrease towards ACOS. This is the pattern expected for interseismic strain due to a locked fault (Fig. 4). However, sites at the northern end of the Nicoya Peninsula show a counterclockwise rotation of the motion vectors to the NW. Significant NW motion of a sliver plate lying between the MAT and the volcanic arc along the Nicaragua Depression extending from northern Costa Rica into El Salvador has long been recognized from earthquake focal mechanisms [White, 1991]. This forearc sliver has been predicted to move at 15 to 20 mm/yr with respect to the Caribbean plate, based on the motion of the Caribbean and Cocos plates and their relative obliquity of convergence [DeMets *et al.*, 1996], and is similar to the 8-13 mm/yr motion predicted by numerical modeling of the plate margin [unpublished manuscript in preparation by P. Lundgren and R. Russo]. Such a secular rate of plate sliver motion would only partially explain the observed horizontal motions. In addition interseismic strain due to strong coupling of the Nicoya segment of the MAT and continued postseismic deformation from the September 1992  $M_w$  7.6 Nicaragua earthquake must also be considered as possible sources of deformation in NW Costa Rica. We will explore these more fully in the next section.

In contrast to NW Costa Rica, the southern half of the country has horizontal motions that move to the ENE relative to the stable Caribbean plate (Fig. 3a). This is the sense of motion expected for

a separate Panama Block, consistent both with the seismicity of the NPDB [Wolters, 1986; Vergara Munoz, 1988], and with the GPS results measured in Panama as part of the CASA project [Trenkamp *et al.*, 1997].

Vertical motions (Fig. 3b) are also found to be significant. In NW Costa Rica where we have 3 sets of measurements (Fig. 3b), several sites on the coast of the Nicoya Peninsula have subsidence rates in excess of 10 mm/yr, transitioning to much smaller vertical rates inland. Generally, vertical GPS solutions have much larger uncertainties than do the horizontal component solutions, caused in large part by atmospheric effects, as well as other possible sources such as misread antenna heights, that most strongly affect the vertical component. Most plate tectonic motions are predominantly horizontal, and large vertical signals are mostly associated with coseismic or postseismic deformation [e.g. Freymueller *et al.*, 1999]. In the case of subduction zones, the coasts along most of these lie greater than 100 km from the trench, resulting in limited vertical interseismic deformation. However, the Nicoya Peninsula extends into the region in which we might expect to find significant interseismic subsidence. Therefore, despite the large errors that exist in the vertical rates for Costa Rica, we have decided to include the vertical signal in our analysis of the Nicoya interseismic deformation and the inversion for the locked portions of the underlying subduction thrust interface. This is motivated by the large constraint that the vertical component has on defining the down-dip extent of locking that can not be matched by the corresponding changes in velocity of the horizontal component. This will be examined further in the following section.

In southeastern Costa Rica the large vertical subsidence is most likely associated with postseismic deformation after the 1991 earthquake. Subsidence is also found for sites closer to the Pacific coast of SE Costa Rica (AGUJ, CAMP, CARA, TIGR). These are suggestive of interseismic deformation due to locking of the MAT thrust. However, the sparseness of these sites, their large vertical uncertainties, and the lack of a clear corresponding pattern in their horizontal velocities (i.e. greater NE motion at the Pacific coast compared to sites inland), preclude a definitive interpretation at this time.

## Seismic Cycle Deformation in the Nicoya Region

The crustal motions in northwest Costa Rica are likely due to the superposition of three main deformations: secular sliver motion of the forearc; postseismic motions continuing after the 1992 Nicaragua earthquake; and interseismic strain along the rest of the MAT, in particular along the seismogenic zone beneath the Nicoya segment. The large subsidence along the Nicoya coast transitioning to uplift further inland appears to fit a simple dislocation model (Fig. 4) for interseismic strain of a partially locked subduction thrust [Savage, 1983; Okada, 1985; Dixon, 1993]. The concept of interseismic deformation at a subduction zone is that the converging oceanic plate (Cocos in this case) subducts at a constant rate. Between earthquakes (interseismic period), the fault is locked and the over riding plate deforms as the subducting plate drags it down and compresses it towards its interior.

In contrast to most other land areas adjacent to subduction zones, the Nicoya Peninsula lies especially close (within 55-60 km) to its trench. Therefore, while most other coastal areas adjacent to trenches lie at or inland from the hinge line (cross-over from interseismic subsidence to uplift), Nicoya juts out well into the much larger amplitude subsidence region. In addition, horizontal velocities of coastal Nicoya sites with respect to ACOS in northern Costa Rica are significant, in keeping with an interseismic source for the observed deformation. An important feature of the Nicoya Peninsula geometry is its potential for discriminating between models of seismogenic coupling. The data in the central Nicoya Peninsula have relatively large subsidence compared to their horizontal motion towards the plate interior, suggesting that the locked portion does not extend close to the trench (Fig. 4). However, there is considerable spatial structure to the horizontal motions that is not easily fit with a simple cross-section model.

To solve for the subduction related seismic deformation in the Nicoya Peninsula region we apply two different numerical inversion algorithms. Each method seeks to solve for a distribution of subfaults with varying slip to best match the GPS observed deformation. Hopefully insight can be gained by examining where the fault slip models are similar and where they differ. As we will show, both methods give similar solutions and suggest that within the limitations of our GPS

solutions and the spatial distribution of sites, and within the intrinsic limitations for surface geodetic measurements to discriminate deformation sources with increasing distance (e.g. depth) from the source, the solutions provide reasonable constraints on the interseismic coupling of the Nicoya subduction segment.

### **Simulated annealing**

First we apply a simulated annealing algorithm [Kirckpatrick *et al.*, 1983], an iterative global minimization approach that uses rectangular elastic half-space Greens functions [Okada, 1985] to solve for multiple dislocations in an elastic half-space. The algorithm we use is based on that of Ihmle [1996] as applied to seismic data and more recently applied to GPS data for the distribution of coseismic slip [Ihmle and Ruegg, 1997]. The simulated annealing algorithm in our application to GPS site vectors solves for the slip of individual subfaults. For this study the fault location and geometry is specified and the parameters we solve for are the dip-slip and strike-slip components of locking. In general, additional parameters can be solved for by simply adding them to the parameter space.

The simulated annealing algorithm is a quasi Monte Carlo approach that iterates to a solution by choosing an evenly distributed random value (0:1) for the slip on a specific parameter (subfault slip) over a specified range of that parameter. For a given iteration, the algorithm loops over the parameter space, changing each parameter one at a time. Each solution is tested, with solutions that reduce the total cost retained, along with occasional solutions that cause an increase in the total cost as determined by a Boltzman probability function criteria according to:

$$r < \exp(-d_c/T)$$

where  $r$  is a random number in the interval (0:1),  $d_c$  is the difference between the new and old total costs, and  $T$  is the “temperature”. At high  $T$  the solution readily accepts new solutions that cause an increase in the cost, allowing the inversion to search for a global minimum. At lower  $T$  only solutions that actually lower the cost are kept and the solution approaches that local minimum. If the starting  $T$  is high enough, and lowered slowly enough, then this local minimum should be a global one. The initial value of  $T$  is determined from an initial selection of a large number of

solutions based on the maximum difference ( $d_c$ ) in these solutions. The temperature is lowered according to:

$$T = T \exp(-\lambda T / \sigma_x)$$

where  $\lambda$  is the cooling speed (set at 0.5 in this study) and  $\sigma_x$  is the standard deviation in the costs of the previous iterations.

At each change of model parameter cost functions are computed. These are quite flexible and are generally of the form:

$$cost_x = \sum (x_{obs} - x_{mod})^2 / \sigma^2$$

where  $cost_x$  is the cost of parameter  $x$  based on the sum of the squared errors divided by the observed sigmas ( $\sigma$ ). Costs can be computed for the data fit; for an *a priori* estimate of the total moment (in the case of an earthquake); and for slip heterogeneity: smoothing can be imposed based on minimizing the gradient between adjacent subfault slip. For purely geodetic data such smoothing is unnecessary since the solutions tend to smooth naturally and for interseismic deformation we do not constrain the total moment. The only cost we impose in this study is for the model and data misfit. We restrict the solution space to not allow the rate of normal slip to exceed the plate convergence rate.

The fault parameters we used are given in Table 2, and consist of an 8x7 mosaic of fault patches, each 30 km long and 20 km wide, forming a 240 x 140 km fault. For the west coast of Costa Rica the marine seismic study of *Ye et al.*, [1996] allows us to define the strike, dip and depth of the thrust interface. The thrust interface dips shallowly towards the coast, increasing to a dip angle of 10 degrees at the central Nicoya coast. From the coast inland the dip is increased to reach a depth of 40 km beneath the axis of the Gulf of Nicoya, based on the depth to seismicity at the top of the subducting slab [M. Protti, personal communication]. The fault model used in this study starts 20 km down-dip from the trench.

#### *Model resolution*

As a first step we test the resolving power of the Nicoya site distribution and the assumed fault geometry by generating a synthetic model for a checkerboard pattern of slip for the fault model

given in Table 2 (Fig. 5a). We solve for both dip-slip and strike-slip fault motion (Fig. 5b,c). To understand the model uncertainty, we run the simulated annealing inversion a number of times, each time using a Gaussian random number generator to vary the inverted simulated GPS data according to each data component's uncertainty. The standard deviation for each fault patch solution is then computed after  $N$  runs (Fig. 5d,e). We find that the most reliable portions of the modeled fault plane are those directly beneath the stations. The solution we find demonstrates that the optimization does a reasonable job beneath the GPS sites but does poorly towards the trench and towards greater depth. Keep in mind that the modeled fault has precisely the same geometry as that which generated the input "data". Other tests in which the fault model was composed of a larger checkerboard were much better resolved. The smaller the fault patch size the more slip is smoothed into neighboring patches. Fault patches located farther from the GPS sites can have relatively large slip that produces a small improvement in the vertical or horizontal fit to a distant site, but without the constraint on amplitude and position that a data point local to that patch would provide. This of course is a well known limitation in geodesy that resolution degrades with distance. On the other hand, locking the entire fault up-dip (towards the trench) from the coastal sites would produce an unacceptable fit to the data (Fig. 4).

#### *Modeling the CORI data*

Early in the analysis it became apparent that there was consistently a residual strike-parallel component of motion (towards the NW) of sites along the interior forearc that was not accounted for by any reasonable models. Since the dislocation model only fits motion associated with fault strain, any secular plate motions would not be expected to be fit by such a model. Therefore, we have removed the SJOS strike-parallel component (7 mm/yr) from all the modeled vectors in NW Costa Rica except ACOS, which lies beyond the volcanic arc and is less affected by forearc sliver motion. To allow for uncertainties in this forearc sliver component, as well as the uncertainty (1-2 mm/yr) in the *Dixon et al.* [1998] Caribbean plate Euler pole relative to the ITRF94, we have added a 3 mm/yr uncertainty to the horizontal GPS vector velocity uncertainties used by both the simulated annealing and SVD inversions.

The best fitting model consists of interseismic deformation from partially locked patches beneath the Nicoya Peninsula (Fig. 6). As with the checkerboard test (Fig. 5), to estimate the uncertainties in the fault model, we make a number of runs (20 in this case) where the data at each iteration consists of the original data plus randomly generated deviations from the original values ( $\delta x$ ,  $\delta y$ ,  $\delta z$ ) that are computed as a normalized (Gaussian) distribution with a standard deviation equal to that of the original data. From these solutions we calculate the standard deviation of each subfault slip component (Fig. 6c,d). The greatest uncertainties generally lie towards the outer side edges of the fault model furthest from the GPS sites, as we found for the test example. A greater amount of uncertainty also lies beneath the inner coast of the Nicoya Peninsula. The fault patches that show the least variation are those directly beneath the SE outer coast of the peninsula, where the high subsidence rates and shallow depth to the fault put the tightest constraints on the solution, and on the fault patches towards the central down-dip edge of the fault where the solution is required to be near zero.

The areas of greatest coupling (most negative dip-slip motion) lie predominantly beneath the outer Nicoya Peninsula, with two other areas located on either end of the modeled fault and further down-dip. These latter fault patches are less reliable as demonstrated by their much higher standard deviations (Fig. 6c).

### **Singular value decomposition**

The second technique we use is the singular value decomposition (SVD), a widely used method for underconstrained inverse problems [Lanczos, 1961; Menke, 1984]. We use the computer program of Larsen [1991] that follows the approach of Harris and Segall [1987]. For this study we have modified the Larsen [1991] SVD inversion software to compute the elastic deformation due to slip on individual fault patches using the equations of Okada [1985], the same used in the simulated annealing inversion.

In applying the SVD approach it is possible to restrict the parameter space by keeping only the  $k$  largest singular values [e.g. Press *et al.*, 1986]. The fit to the data and the variance of the model depend on the number of  $k$  retained. Few  $k$  result in lower model variance (i.e. smoother fault slip)

at the expense of a poorer fit to the data. For high resolution fault models the *Larsen* [1991] algorithm can avoid oscillatory patterns in the slip distribution by applying smoothing constraints over the model null space by considering quasi data [*Snay*, 1989].

We apply the SVD inversion using the same fault geometry used for the simulated annealing inversion (Table 2). This particular solution (Fig. 7) was computed for  $k = 30$ , although models with  $k < 5$  produced very similar slip distributions, particularly for the dip-slip component beneath the central Nicoya coast. Thus, the model vectors match the data fairly well at the expense of greater slip heterogeneity. This is most visible in the strike-slip solution where the solution is close to zero in general. However, even at very low  $k$  values, the central area of the dip-slip solution was robust, with the smaller singular values (higher  $k$ 's) refining the fit, especially for sites at the margins of the GPS network. In general the SVD solutions are most sensitive to areas on the fault nearest the data. This is not surprising given the subfault dimensions with respect to the GPS site spacing, and the spatial geometry of sites nearest the trench where the fault plane lies nearly horizontal beneath them at a shallow depth of 10-15 km.

Not surprisingly, the dip-slip component is more pronounced. It defines an area roughly coincident with the Nicoya Peninsula, generally at 25-75% coupling, but with two strongly coupled patches beneath the central outer coast of the peninsula (Fig. 7a).

### **Simulated Annealing vs. SVD models**

We applied two different inverse methods that resulted in similar models. Both of these models solved for the deformation due to a dislocation buried in an elastic halfspace [*Okada*, 1985]. In this regard the models are directly comparable, but the presence of significant crustal structural heterogeneity would be expected to modify our results. To this end more sophisticated modeling would be required (e.g. finite element or other numerical modeling techniques), and is beyond the scope of this paper.

The models derived with the SVD and simulated annealing inversions all had several features in common. What is modeled as either strike-slip or normal fault motion on the fault plane represents the deformation resulting from partially locked patches on the subduction thrust interface [i.e.

*Savage, 1983*]. Therefore, for a patch with a dip-slip motion computed as -86 mm/yr (normal motion), this is equivalent to 100% locking on that patch for a convergence rate of 86 mm/yr. Positive strike-slip motion is right-lateral (RL) in this model. Negative, left-lateral (LL), values correspond to locked patches moving towards the NW with the slightly oblique motion of the Cocos plate, while RL motion would represent creep of the over riding plate towards the SE. For the representative model (Figures 6b,7b) the strike-slip component is fairly heterogeneous, with one area of RL motion found beneath the SE end of the Nicoya Peninsula, while LL patches are more randomly scattered. Since we have already removed the 7 mm/yr sliver motion we are assuming slip partitioning due to oblique subduction. As a long-term kinematic model slip partitioning can provide only a partial explanation where crustal deformation on short time scales is dependent on the coupling across the subduction and interior strike-slip fault zones. Models in which the LL trench parallel component for site SJOS was not removed had a strong LL patch beneath the entire Nicoya Peninsula consistent with the oblique subduction and coupling of the thrust fault.

For both inversions the areas of greatest locking generally located beneath the outer coast of the Nicoya Peninsula. Partly this reflects the limited distribution of our GPS sites, but certain features such as the high coupling beneath the SE outer coast of the peninsula and, conversely, the requirement of little coupling beneath the inner coast of the peninsula are features evident in the GPS data. The GPS vertical signal is especially critical in these solutions. The much greater uncertainty in the vertical GPS means that the details of the locking pattern, particularly its down-dip extent, are strongly dependent on sites located in the transition from subsidence along the outer coast to uplift towards the interior. The large amplitude of the vertical signal on the outer coast relative to the magnitude of the horizontal vectors restricts the amount of locking allowed towards the trench.

Comparing and contrasting these two models suggests that we are beginning to get an understanding of the seismic coupling heterogeneity beneath the Nicoya Peninsula. A greater

density of sites within the Nicoya Peninsula would help improve the resolution of the slip heterogeneity.

## **Discussion and Conclusions**

Preliminary GPS results from Costa Rica show a varied signal that is the summation of several sources due to fundamentally different processes operating on differing time scales. Future measurements across the entire network will allow us to extend the modeling of the MAT further south, better constraining its seismic hazard, and will allow a quantitative assessment of postseismic effects following the 1991 Limon earthquake beneath the entire southern half of the country. The modeling results for the Nicoya region demonstrate the limitations of the current network. A greater number of sites, both along the strike of the MAT and in the density of sites in areas such as the Nicoya Peninsula, and the number of measurement episodes, are needed to better define the properties of the seismogenic zone. Greater site density would provide important data strength and allow a higher resolution of the slip heterogeneity across the thrust interface.

Several limitations with the current data set deserve further comment. The first regards the vertical GPS solutions. As evident in GPS time series (Fig. 2), several sites on the Nicoya peninsula show patterns of deformation that do not fit a perfectly straight line after three sets of occupations. These sites include ACOS, SAMA (possibly), SJUA, MATA, and to a lesser extent PAQU. In the case of ACOS the 1996 data appear higher than a line connecting 1994-1997 would predict, while for the subsiding sites such as SJUA, the apparently fast subsidence from 1994-1996 was non-existent from 1996-1997. This pattern appears most evident along the coast and is possibly due to atmospheric conditions that were different in one of the campaigns for example. Sites SAMA, SJUA, PAQU, and JICA, had normal dry season conditions in 1997, whereas MATA, GRAN, GUAR, and BALL were occupied during a week of high humidity and scattered thunderstorms. This was particularly evident in the MATA and GRAN vertical data where there was a larger amount of scatter in the daily solutions than usual. In 1994 and 1996 the data were collected in the middle of the dry season.

A second limitation lies with the horizontal motions used to model the fault. The conversion to the Caribbean fixed reference frame and the removal of a trench parallel component both have their uncertainties. We have attempted to include these uncertainties in the modeling. The error in the forearc motion would mostly affect the strike-slip component of the fault model. The conversion of the horizontal vectors to a Caribbean frame fits well with the small trench perpendicular motion that is left at site ACOS.

Steady-state plate margin deformation is apparent (Fig. 3b) along the forearc sliver of NW Costa Rica at a rate around 7 mm/yr based on the component of arc-parallel motion that was not readily modeled as interseismic deformation. This is not a very satisfying way of arriving at an estimate of the forearc motion, but even with more data from sites distributed along the entire forearc through Nicaragua any estimation of this motion by geodesy will necessarily rely on separating out a component of seismic cycle slip, either due to a strike-slip component on the seismogenic interface, or due to effects from adjacent segments with different amounts of coupling.

In southern Costa Rica we find E-NE motion of the Panama Block with respect to the Caribbean plate proper. However, here too there are significant seismic cycle contributions to the secular motions that hinder a unique solution. The southern half of Costa Rica features both interseismic strain from subduction beneath its Pacific coast and postseismic deformation following the 1991 Limon earthquake beneath its Caribbean coast. Sites along the SE Caribbean coast of Costa Rica have very low horizontal velocities relative to the stable Caribbean plate compared to sites further inland. In contrast these sites have large vertical rates suggesting either large interseismic strain from the thrusts of the NPDB or postseismic deformation continuing after the 1991 Limon earthquake. We are waiting to remeasure these sites in the future before discriminating between models. An interseismic signal should be steady-state, whereas any postseismic signal should be time dependent. One unresolved issue that arose from GPS measurements collected after the Limon earthquake in 1991 was the vertical discrepancy between the GPS measured uplift at LIMO (16 cm) by *Lundgren et al.* [1993] ~70 days after the earthquake, leveling data (23 cm) ~50 days after

the earthquake [*DeObaldia et al.*, 1991], and the 60-80 cm of coastal uplift adjacent the LIMO site measured by *Plafker and Ward* [1992] approximately 2 weeks following the earthquake. Rapid postseismic afterslip such as that measured with GPS immediately following the 1995 Jalisco earthquake by *Melbourne et al.* [manuscript in preparation] suggests that a similar postseismic process may have been active following the 1991 Limon earthquake.

In NW Costa Rica the GPS observations fit a model of heterogeneous seismic coupling with individual fault patches beneath the central and southeast Nicoya Peninsula having the highest amount at more than 80% locked assuming a convergence rate of 86 mm/yr. The deformation pattern we find in NW Costa Rica has many similarities with recent observations from Sumatra [*Prawirodirdjo et al.*, 1997] and the central Andes [*Norabuena et al.*, 1998]. In those studies only horizontal GPS motions were used to estimate dislocation model parameters and the observed deformation patterns could be fit with a combination of interseismic strain partitioning between the trench and an interior fault system.

Despite the current solution set's limitations, particularly with regard to the vertical uncertainties, an important step can be made toward defining the slip distribution along the seismogenic zone (Figs. 6,7). An important part of this is due to the significant vertical signal measurable with episodic GPS observations to which the dislocation models are particularly sensitive. In this regard the Nicoya Peninsula, by lying directly above the seismogenic zone (10-20 km beneath) in a location of fast convergence is uniquely suited to defining the slip distribution across the subduction thrust interface. Additional measurements and densification of the network would allow greater resolution of this heterogeneity. Such a detailed map of seismic coupling when combined with a future large thrust earthquake will provide important insight into the relation between interseismic coupling and the nucleation of large subduction zone earthquakes and the slip potential for future earthquakes.

**Acknowledgments.** We would like to thank all the people who have provided their invaluable help in carrying out the GPS field work: J. Richardson, J. Ulate, T. Marino, F. DeObaldia, R. van der Laat, M. Smith, P. Sak, G. Liu, B. O'Neill, E. Malavassi, and the many students who have

participated from the Universidad Nacional and from the Escuela de Topografia y Catastro y Geodesia. We also received much help from UNAVCO, and G. Lyzenga for providing GPS receivers and supporting equipment. We thank T. Melbourne for providing the SVD inversion code and P. Ihmle for providing a FORTRAN version of his simulated annealing code. We also thank the detailed comments of two anonymous reviewers. This work was carried out at the Jet Propulsion Laboratory, California Institute of Technology, under contract with the National Aeronautics and Space Administration.

## REFERENCES

- Argus, D., and M. Heflin, Plate motion and crustal deformation estimated with geocentric data from the Global Positioning System, *Geophys. Res. Lett.*, 22, 1973-1976, 1995.
- Blewitt, G., Carrier phase ambiguity resolution for the Global Positioning System applied to geodetic baselines up to 2000 km, *J. Geophys. Res.*, 94, 10,187-10,203, 1989.
- DeMets, C., R. G. Gordon, D. F. Argus, and S. Stein, Effects of recent revisions to the geomagnetic reversal time scale on estimates of current plate motions, *Geophys. Res. Lett.*, 21, 2191-2194, 1994.
- DeMets, C., T. Dixon, F. Farina, E. Calais, P. Jansma, and P. Mann, GPS-derived velocities in the northeastern Caribbean: Implications for Caribbean-North America motion and the NUVEL-1A model, *EOS, Trans. Amer. Geophys. Un.*, Fall Meeting Supplement, F143, 1996.
- DeObaldia, F., T. Marino, R. Van der Laat, F. Hernandez, E. Malavassi, and K. McNally, Coseismic uplift associated with the Costa Rica earthquake ( $M_s$  7.5) of April 22, 1991, *EOS, Trans. Amer. Geophys. Un.*, 72, 301, 1991.
- Dixon, T. H., GPS measurements of relative motion of the Cocos and Caribbean plates and strain accumulation across the Middle America trench, *Geophys. Res. Lett.*, 20, 2167-2170, 1993.
- Dixon, T. H., F. Farina, C. DeMets, P. Jansma, P. Mann, and E. Calais, Relative motion between the Caribbean and North American plates and related boundary zone deformation from a decade of GPS observations, *J. Geophys. Res.*, 103, 15,157-15,182, 1998.

- Donnellan, A., and G. A. Lyzenga, GPS observations of fault afterslip and upper crustal deformation following the Northridge earthquake, *J. Geophys. Res.*, *102*, 21,285-21,297, 1998.
- Freymueller, J. T., S. C. Cohen, and H. J. Fletcher, Spatial variations in present-day deformation, Kenai Peninsula, Alaska, and their implications, *J. Geophys. Res.*, submitted, 1999.
- Harris, R. A., and P. Segall, Detection of a locked zone at depth on the Parkfield segment of the San Andreas fault, *J. Geophys. Res.*, *92*, 7945-7962, 1987.
- Heflin, M., W. Bertiger, G. Blewitt, A. Freedman, K. Hurst, S. Lichten, U. Lindqwister, Y. Vigue, F. Webb, T. Yunck, and J. Zumberge, Global geodesy using GPS without fiducial sites, *Geophys. Res. Lett.*, *19*, 131-134, 1992.
- Ihmlé, P. F., Monte Carlo slip inversion in the frequency-domain: Application to the 1992 Nicaragua slow earthquake, *Geophys. Res. Lett.*, *23*, 913-916, 1996.
- Ihmlé, P. F., and J.-C. Ruegg, Source tomography by simulated annealing using broad-band surface waves and geodetic data: Application to the Mw = 8.1 Chile 1995 event, *Geophys. J. Int.*, *131*, 146-158, 1997.
- Kanamori, H., and M. Kikuchi, The 1992 Nicaragua earthquake: A slow tsunami earthquake associated with subducted sediments, *Nature*, *361*, 714-716, 1993.
- Lanczos, C., Linear Differential Operators, D. Van Nostrand, New York, 1961.
- Larsen, S. C., Geodetic measurements of deformation in southern California, Ph.D. thesis, California Institute of Technology, pp. 351, 1991.
- Lichten, S. M., and J. S. Border, Strategies for high-precision Global Positioning System orbit determination, *J. Geophys. Res.*, *92*, 12,751-12,762, 1987.
- Lundgren, P. R., S. Kornreich Wolf, M. Protti, and Kenneth J. Hurst, GPS measurements of crustal deformation associated with the 22 April 1991, Valle de la Estrella, Costa Rica Earthquake, *Geophys. Res. Lett.*, *20*, 407-410, 1993.

- Mann, P., C. Schubert, and K. Burke, Review of Caribbean neotectonics; and neotectonic map of the Caribbean region, *in* The Caribbean region; The Geology of North America, G. Dengo and J. E. Case, Eds., Geological Society of America, v. H., 307-338, Plate 11, 1990.
- Marshall, J. S., and R. S. Anderson, Quaternary uplift and seismic cycle deformation, Peninsula de Nicoya, Costa Rica, *Geol. Soc. Am. Bull.*, 107, 463-473, 1995.
- Menke, W., Geophysical Data Analysis: Discrete Inverse Theory, Academic, Orlando, Fla., 1984.
- Norabuena, E., L. Leffler-Griffin, A. Mao, T. Dixon, S. Stein, I. S. Sacks, L. Ocala, and M. Ellis, Space geodetic observations of Nazca-South America convergence across the central Andes, *Science*, 279, 358-362, 1998.
- Okada, Y., Surface deformation due to shear and tensile faults in a half-space, *Bull. Seismol. Soc. Amer.*, 75, 1135-1154, 1985.
- Piatanesi, A., S. Tinti, and I. Gavagni, The slip distribution of the 1992 Nicaragua earthquake from tsunami run-up data, *Geophys. Res. Lett.*, 23, 37-40, 1996.
- Plafker, G., and S. N. Ward, Backarc thrust faulting and tectonic uplift along the Caribbean Sea coast during the April 22, 1991 Costa Rica earthquake, *Tectonics*, 11, 709-718, 1992.
- Prawirodirdjo, L., Y. Bock, R. McCaffrey, J. Genrich, E. Calais, C. Stevens, S. S. O. Puntodewo, C. Subarya, J. Rais, P. Zwick, and Fauzi, Geodetic observations of interseismic strain segmentation at the Sumatra subduction zone, *Geophys. Res. Lett.*, 24, 2601-2604, 1997.
- Press, W. H., B. P. Flannery, S. A. Teukolsky, and W. T. Vetterling, Numerical Recipes in C, Chapter 10, Cambridge University Press, Cambridge, 1988.
- Protti, M.; and Schwartz, S.; Mechanics of back arc deformation in Costa Rica: Evidence from an aftershock study of the April 22, 1991, Valle de la Estrella, Costa Rica, earthquake ( $M_w=7.7$ ); *Tectonics*, Vol. 13, No. 5, p. 1093-1107, 1994.
- Protti, M., K. McNally, J. Pacheco, V. Gonzalez, C. Montero, J. Segura, J. Brenes, V. Barboza, E. Malavassi, F. Guendel, G. Simila, D. Rojas, A. Valesco, A. Mata, and W. Schillinger, The March 25, 1990 ( $M_w=7.0$ ,  $M_L=6.8$ ), earthquake at the entrance of the Nicoya Gulf, Costa Rica:

- Its prior activity, foreshocks, and triggered seismicity, *J. Geophys. Res.*, **100**, 20,345-20,358, 1995.
- Protti, M.; Guendel, F.; and McNally, K.; Correlation between the age of the subducting Cocos Plate and the geometry of the Wadati-Benioff zone under Nicaragua and Costa Rica. In P. Mann (Editor), *Geologic and Tectonic Development of the Caribbean Plate Boundary in Southern Central America*. Geol. Soc. Am. Special Paper 295, 309-326, 1995.
- Savage, J. C., A dislocation model of strain accumulation and release at a subduction zone, *J. Geophys. Res.*, **88**, 4984-4996, 1983.
- Snay, R. A., Enhancing the geodetic resolution of fault slip by introducing prior information, *Manuscripta Geodaetica*, **14**, 391-403, 1989.
- Trenkamp, R., J. N. Kellogg, and J. T. Freymueller, Kinematics of the Panama arc - South America collision, *EOS, Trans. Amer. Geophys. Un.*, Fall Meeting Supplement, F167-F168, 1997.
- Vergara Munoz, A., Tectonic pattern of the Panama Block deduced from seismicity, gravitational data and earthquake mechanisms: implications for the seismic hazard, *Tectonophysics*, **154**, 253-267, 1988.
- Webb, F., and J. Zumberge, editors, *An introduction to GIPSY/OASIS II*, JPLM D-11088, Jet Propulsion Laboratory, California Institute of Technology, 1995.
- White, R. A., Tectonic implications of upper-crustal seismicity in Central America, in Slemmons, D. B., Engdahl, E. R., Zoback, M. D., and Blackwell, D. D., eds., *Neotectonics of North America*, Boulder, Colorado, Geol. Soc. Am., Decade Map Vol. 1., 323-328, 1991.
- Wolters, B., Seismicity and tectonics of southern Central America and adjacent regions with special attention to the surroundings of Panama, *Tectonophysics*, **128**, 21-46, 1986.
- Ye, S., J. Bialas, E. R. Flueh, A. Stavenhagen, R. von Huene, G. Leandro, and K. Hinz, Crustal structure of the Middle American Trench off Costa Rica from wide-angle seismic data, *Tectonics*, **15**, 1006-1021, 1996.

Zumberge, J., M. Heflin, D. Jefferson, M. Watkins, and F. Webb, Precise point positioning for the efficient and robust analysis of GPS data from large networks, *J. Geophys Res.*, 102, 5005-5017, 1997.

**Table 1.** GPS site locations and their calculated rates and rms errors (relative to the CA plate).

Site ID	Latitude	Longitude	North (mm/yr)	North error	East (mm/yr)	East error	Vertical (mm/yr)	Vertical error
ACOS	10.54	275.39	3.99	0.83	2.77	1.39	4.13	4.20
AGUJ	9.72	275.37	8.39	1.89	-2.09	2.98	-15.96	9.76
BALL	10.38	274.55	11.08	1.36	-2.77	1.87	-1.41	6.77
BRAT	9.55	277.10	8.23	1.97	13.95	3.15	-27.18	10.01
CABU	10.13	275.22	7.52	0.97	1.25	1.44	0.41	4.82
CAMP	8.63	277.16	7.31	1.91	12.00	3.34	-23.12	9.46
CARA	8.44	276.53	25.33	2.75	19.27	5.50	-8.19	14.62
CRUZ	11.05	274.36	7.76	1.60	-5.89	2.16	-0.29	7.75
ETCG	9.99	275.89	8.08	1.52	7.53	2.92	0.63	8.03
GRAN	10.56	274.34	9.96	1.31	-2.30	1.76	-3.43	6.39
GUAR	10.14	274.55	16.46	1.30	7.13	2.03	8.76	6.63
JICA	9.97	274.86	9.22	1.01	6.88	1.47	-1.18	5.02
LIBE	10.65	274.57	14.08	1.29	-3.43	1.91	1.17	6.58
LIMO	9.96	276.97	-0.52	1.62	8.09	2.38	-28.61	8.02
MANZ	9.61	277.32	9.61	3.13	9.63	5.71	-5.07	15.83
MATA	10.35	274.18	9.00	1.46	-1.03	2.26	-10.01	7.62
PAQU	9.83	275.04	9.83	1.12	5.20	1.85	7.38	5.96
SAMA	9.88	274.45	22.85	0.98	6.95	1.54	-27.51	5.21
SJOS	10.36	275.05	5.19	2.12	-4.87	3.81	7.29	10.94
SJUA	10.06	274.24	11.33	1.42	8.56	1.99	-9.26	6.88
TIGR	9.04	276.70	25.52	3.34	23.97	4.45	-16.62	17.62
VUEL	9.62	276.14	15.32	2.06	9.46	3.71	31.45	10.31
ZUMA	9.65	274.91	7.67	2.16	-0.76	3.39	-24.05	10.68

**Table 2.** Top, center location of each row of model fault patches.

Row	Lat.	Lon.	Depth (km)	Dip (degrees)
1	9.709	-85.923	5.0	8
2	9.851	-85.805	7.8	10
3	9.993	-85.688	11.9	15
4	10.136	-85.570	20.5	25
5	10.278	-85.453	38.8	25
6	10.420	-85.335	47.2	25
7	10.562	-85.218	55.7	25

## Figures

**Fig. 1.** Tectonic map of Costa Rica. Solid circles, locations of  $M > 7$  earthquakes of this century and their year; black triangles, active volcanoes; gray shading shows the water depth and continuous lines the depth to the seismogenic slab in km (*Protti et al.*, 1995b); NPDB: North Panama Deformed Belt; dashed lines perpendicular to the Middle American Trench delineate thrust segments; dashed lines from the city of Limon across central Costa Rica represent the transcurrent northern boundary zone of the Panama Block.

**Fig. 2.** GPS time series for sites in the Nicoya region of NW Costa Rica. Each point represents a single day position with the scaled formal error given by the vertical line (scale factor 3.67). Solutions for different sites have been offset, tick marks are at 1 cm intervals. Station codes correspond to sites shown in Fig. 3a.

**Fig. 3.** GPS solutions. White arrows show relative Cocos-Caribbean plate convergence vectors. (a) Vertical rates with station codes labeled. (b) Horizontal velocities with respect to the fixed Caribbean plate model of *Dixon et al.*, [1998].

**Fig. 4.** Theoretical dislocation models after *Okada* [1985]. (a) Vertical deformation as a function of distance perpendicular to the trench. Dashed curve is for a fully locked thrust from the trench for a distance of 95 km down-dip, shown as the dashed portion of the thrust in (c). Solid gray curve is for a short (25 km) locked segment from 70-95 km down-dip (solid gray segment in panel (c)). (b) Horizontal surface motions expected for each of the models shown in (c) relative to the plate interior. In each panels (a) and (b) the vertical and trench perpendicular components of the GPS velocities for the sites in the Nicoya region are plotted with their 1 sigma errors. The gray curve shows that for a short locked segment a reasonable fit to the first order deformation pattern is obtained: a large amplitude vertical subsidence at the Nicoya coast with a relatively low horizontal motion in comparison.

**Fig. 5.** Sensitivity test of the simulated annealing inversion. (a) Input checkerboard pattern of slip on the thrust fault, black patches corresponding to a rate of 83 mm/yr of normal slip, gray patches with 0 slip. (b) Dip-slip component of the inverted slip. Arrows show the vertical simulated data (black) with the solved for vectors shown in white. (c) Strike-slip component of the inverted fault slip. Arrows show the simulated data (black) and solved for horizontal vectors (white). (d) Standard deviation in the inverted dip-slip component, (e) standard deviation for the strike-slip component.

**Fig. 6.** Simulated annealing inversion of the GPS solutions for NW Costa Rica. (a) Dip-slip component of the fault slip. Arrows show the observed (black) and inverted (white) vertical components. (b) Strike-slip component of the fault slip. Arrows show horizontal observed (black) and inverted (white) vectors. (c) Standard deviation in the dip-slip component, (d) standard deviation in the strike-slip component.

**Fig. 7.** Interseismic model derived using the SVD algorithm. (a) Dip-slip component of the inverted fault slip. Arrows show the vertical component of the observed and inverted velocities (same convention as in Fig. 6). (b) Strike-slip component of the inverted fault slip. Arrows show the horizontal observed and inverted site velocities. (c) and (d) show the standard deviations in the dip-slip and strike-slip fault components, respectively.

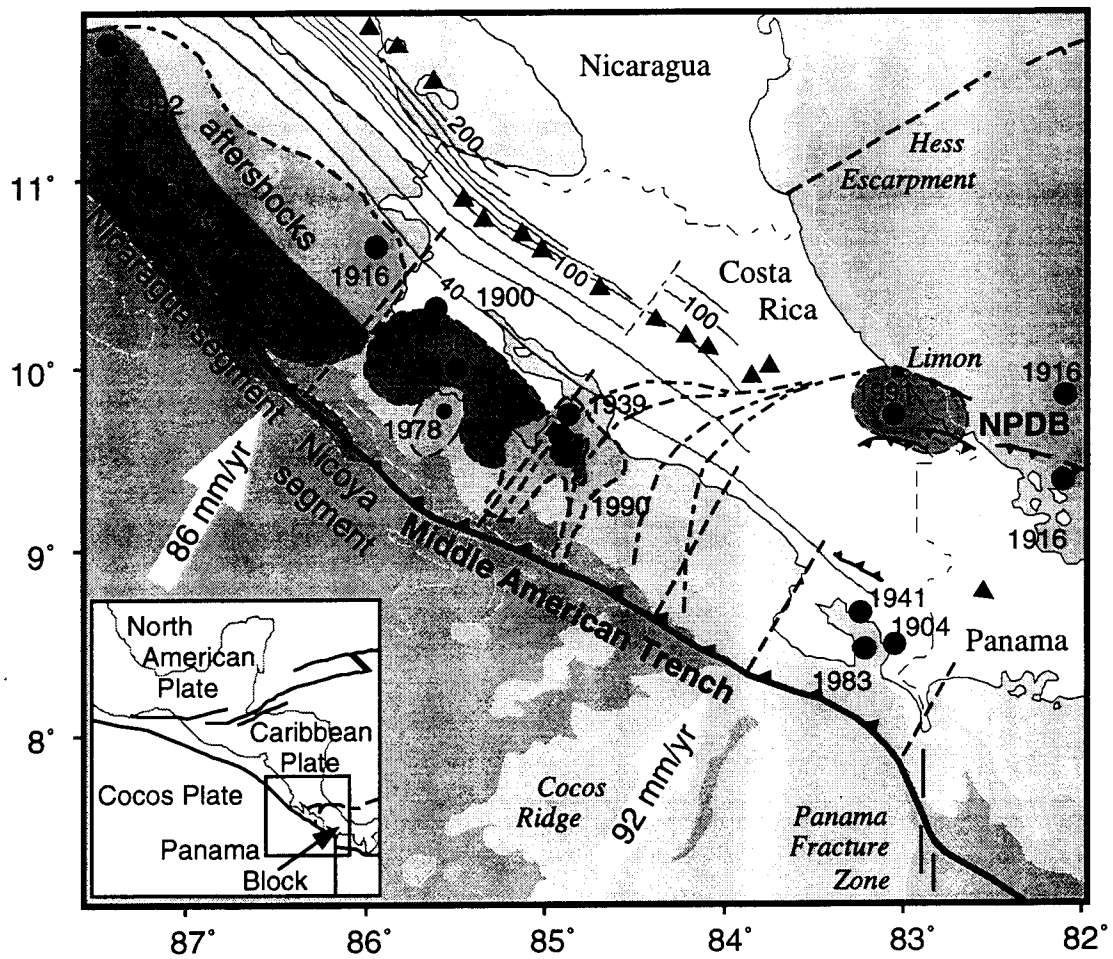


Figure 1

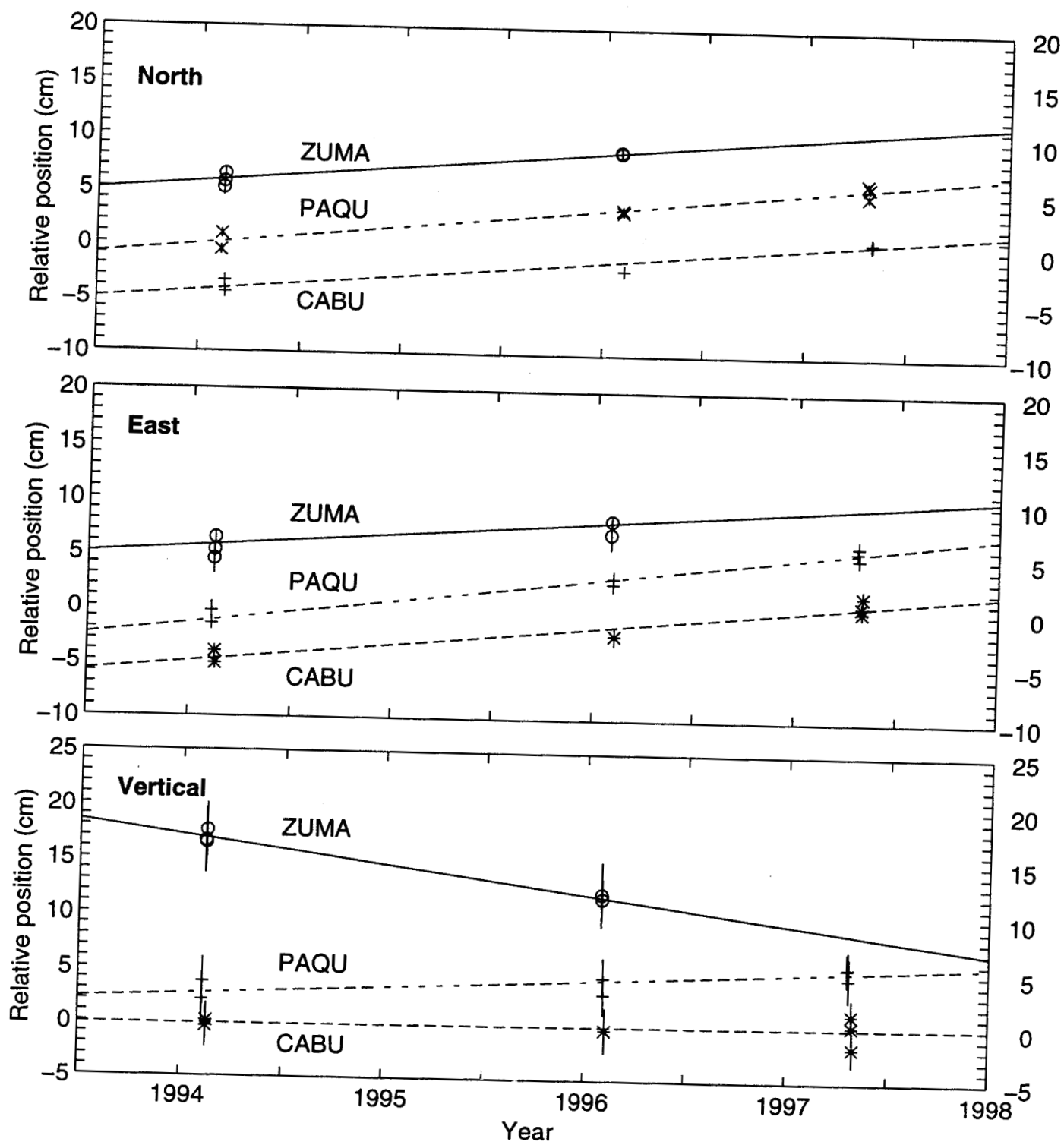


Figure 2a

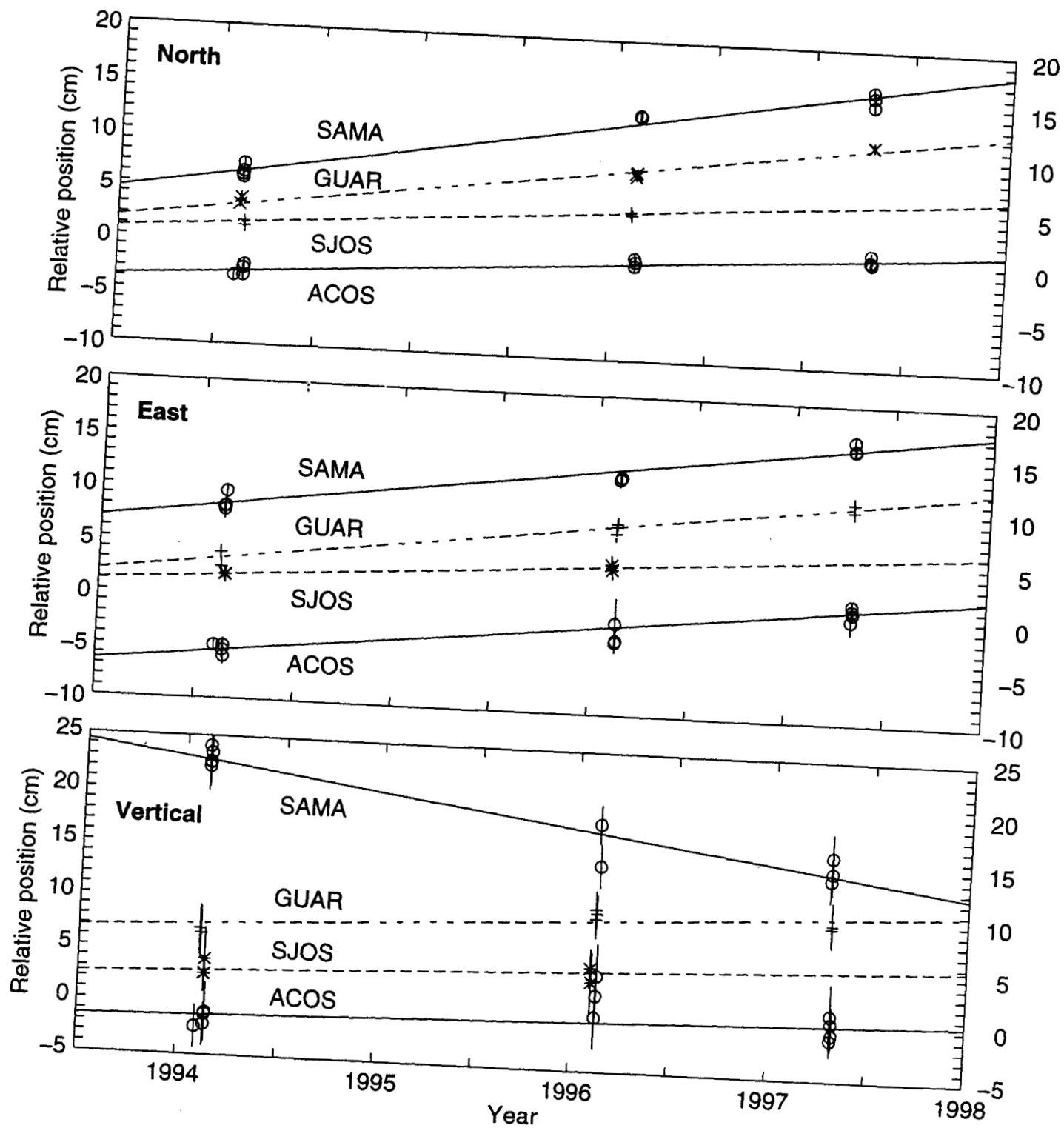


Figure 2b

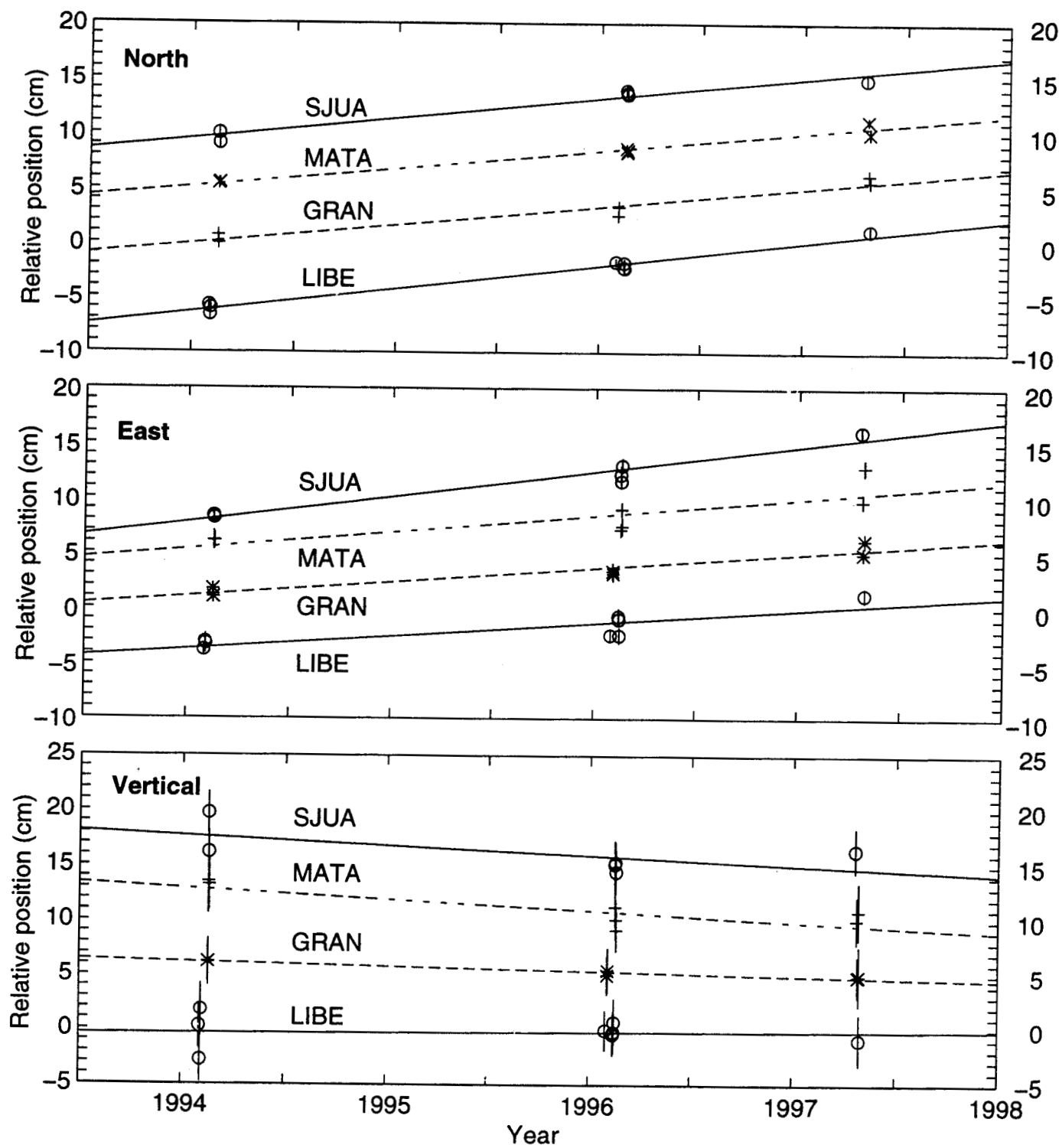


Figure 2c

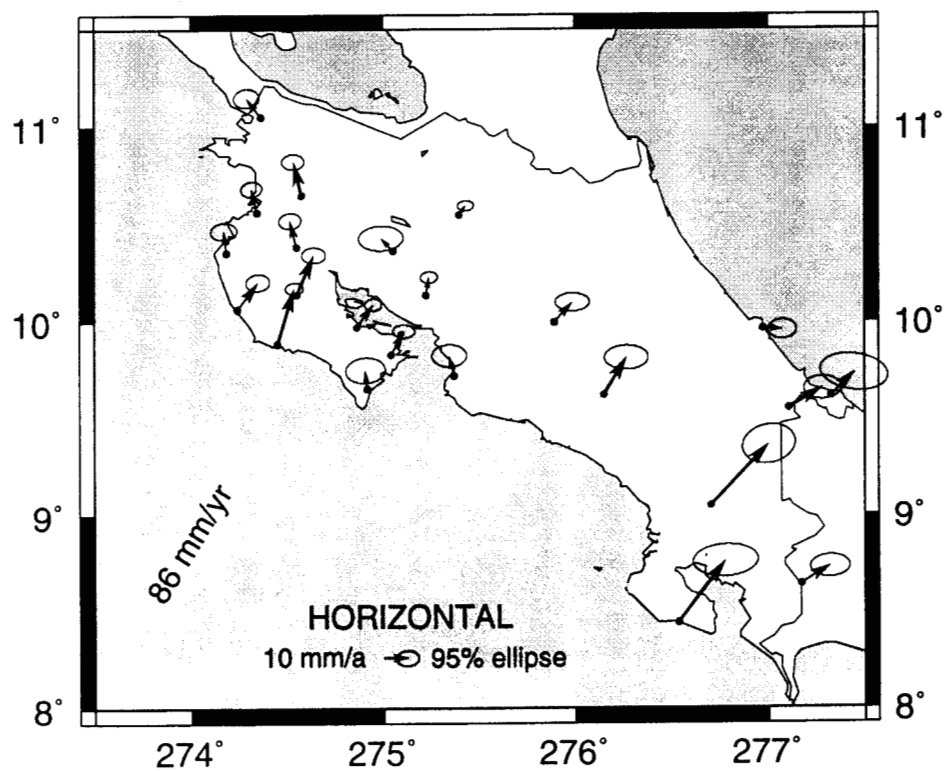
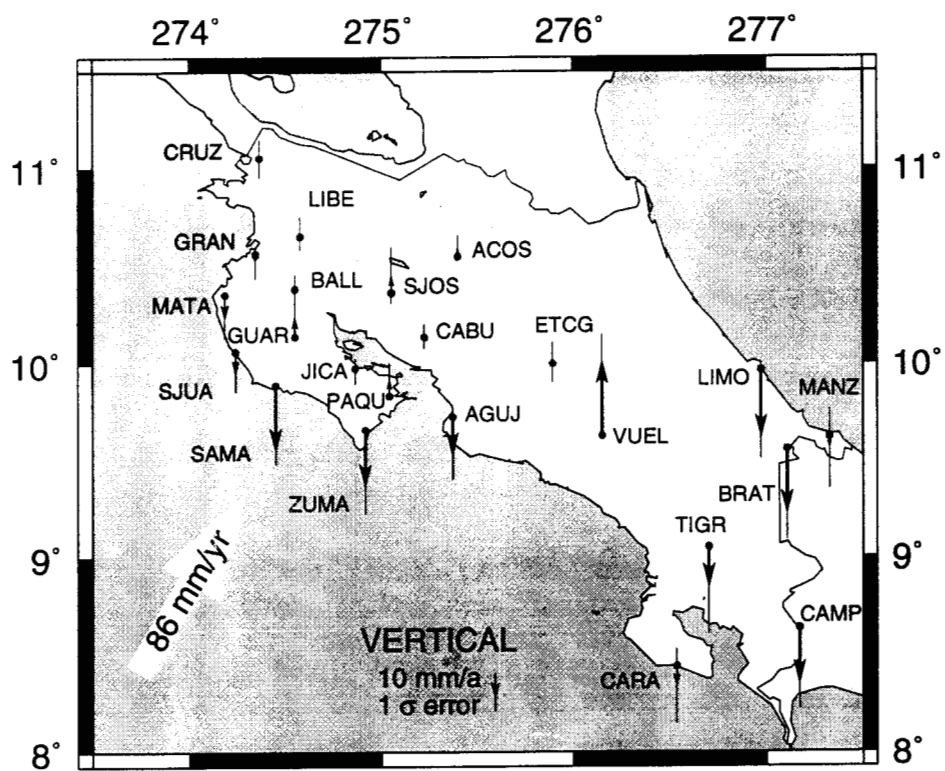


Figure 3

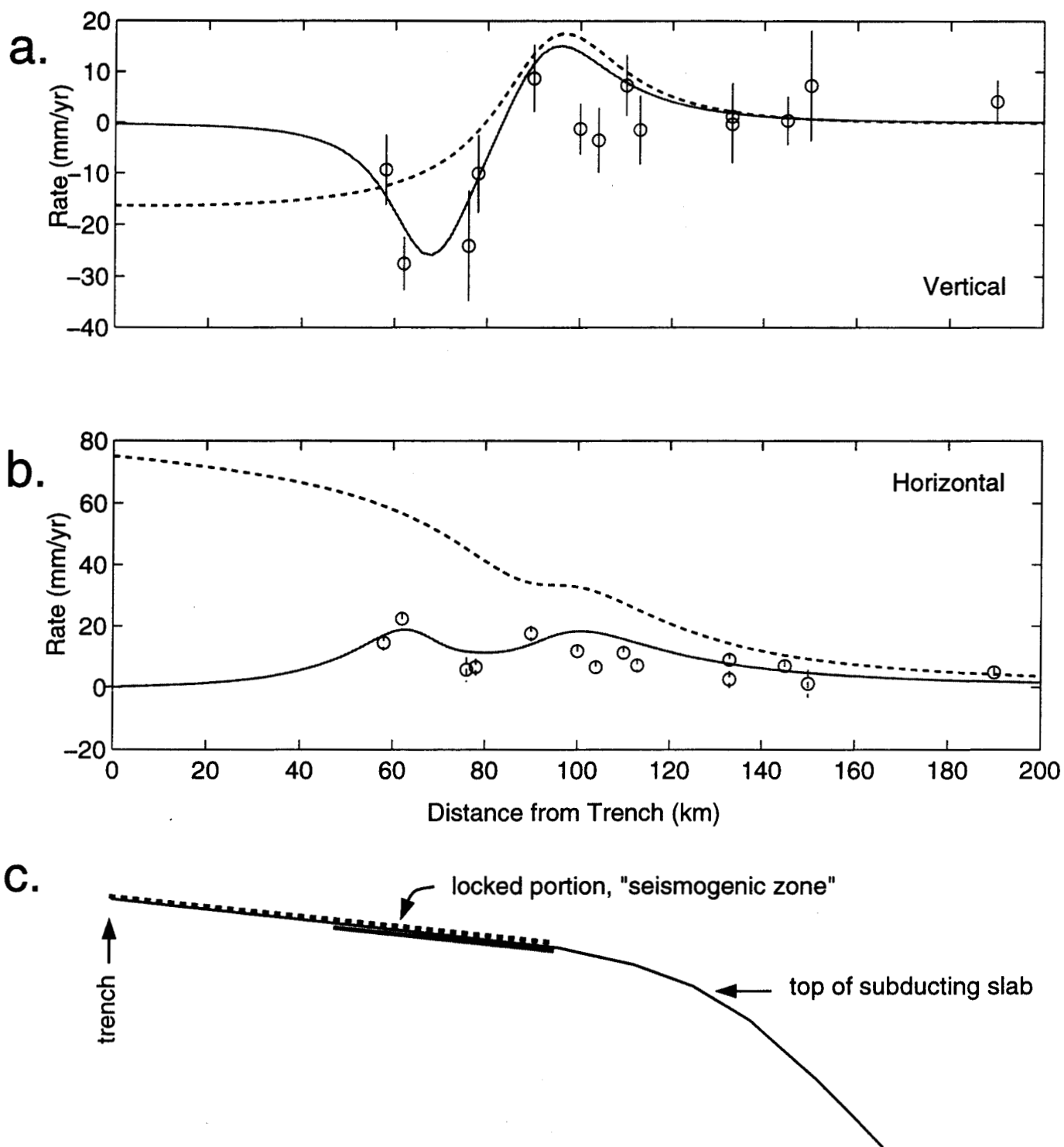


Figure 4

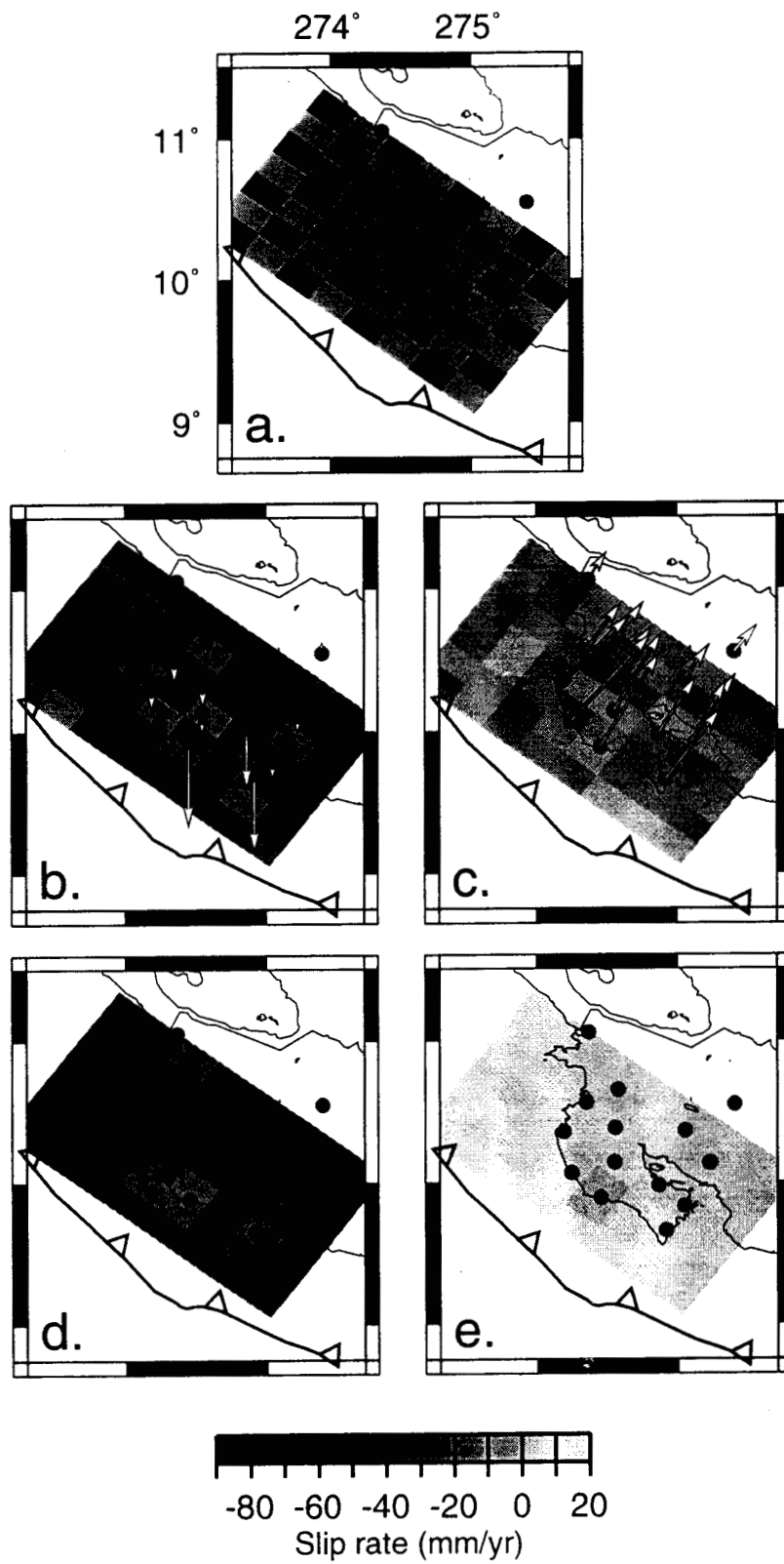


Figure 5

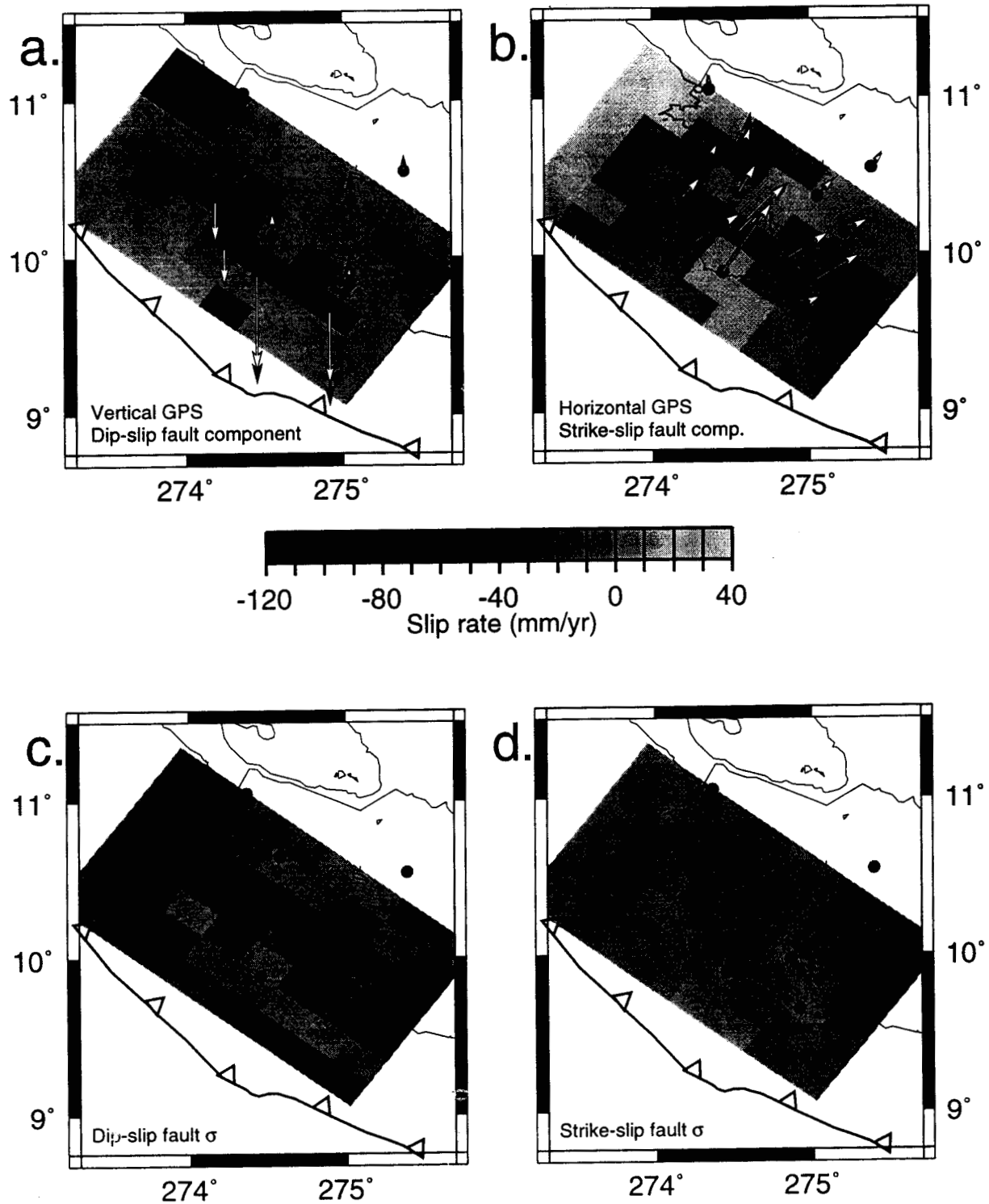


Figure 6

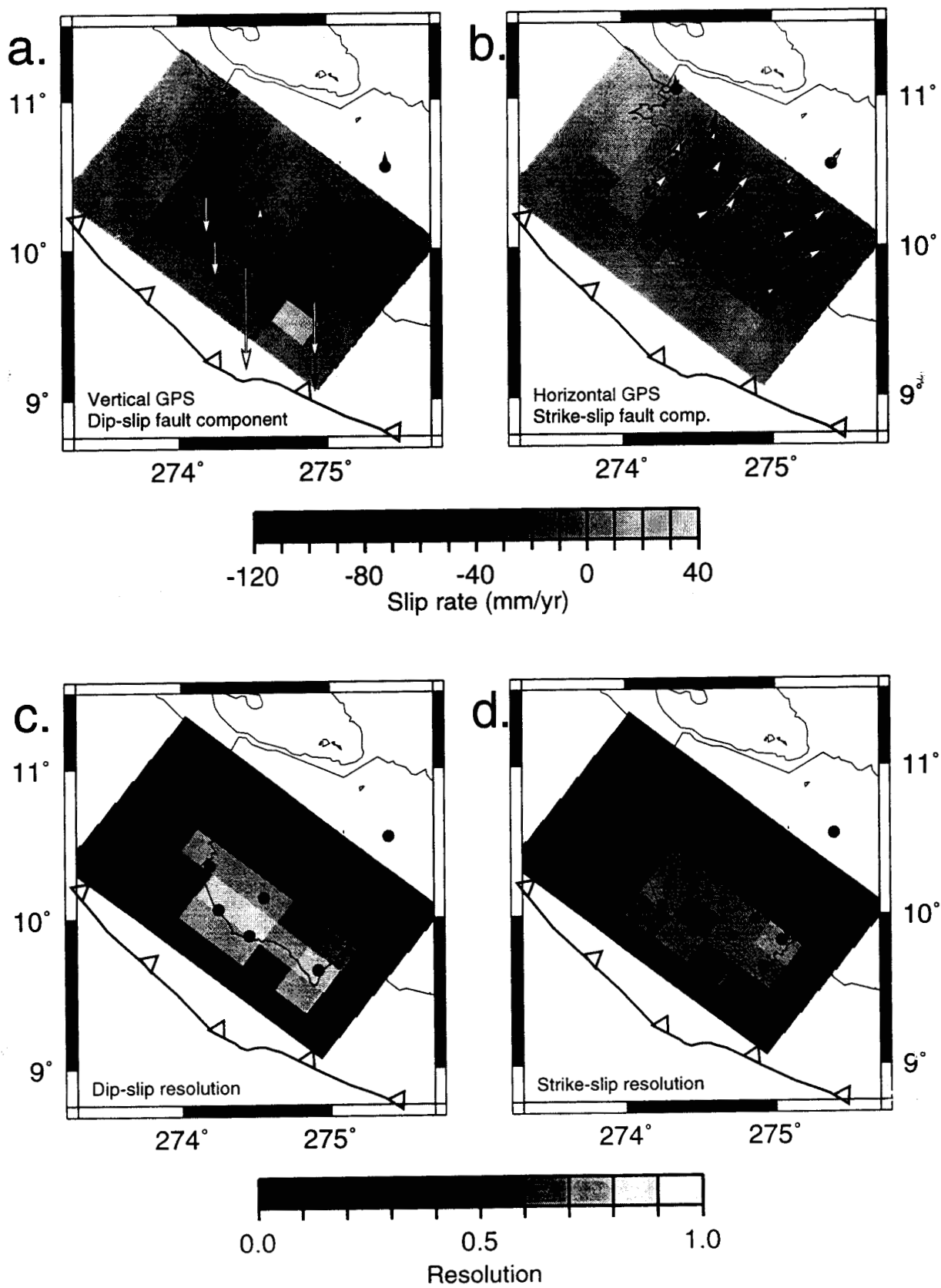


Figure 7